Journal of Applied Fluid Mechanics, Vol. 18, No. 1, pp. 171-190, 2025.
Available online at www.jafmonline.net, ISSN 1735-3572, EISSN 1735-3645.
https://doi.org/10.47176/jafm.18.1.2765

Parametric Analysis of Cooling of Air Inside a Ventilated Enclosure - A Convenient Solution to Achieve *Single Room Multiple Thermal Zones* for Indoor Farming

A. D. Chaudhari[1], P. Bhupathi[2] and V. V. Joshi[1†]

[1] *School of Mechanical Engineering, VIT Vellore, Tamilnadu, 632014, India*
[2] *VIT School of Agricultural Innovations and Advanced Learning, VIT Vellore, Tamilnadu, 632014, India*

†Corresponding Author Email: vijesh.joshi@vit.ac.in

ABSTRACT

This paper explores the potential of a cylindrical enclosure with vent holes to create and maintain the desired thermal environment for indoor farming. Different thermal zones can be made in a single room when such enclosures are used in multiple numbers in a single room. A comparative analysis of twelve different air cooling/heating configurations was conducted. Each cylindrical enclosure is air-filled, with two heat sinks facing each other and vent holes in the top and bottom surfaces. Six configurations had heat sinks oriented vertically, and the other six had heat sinks inclined at 45°. These configurations (vertical and inclined heat sinks) have been studied for different heat sink temperatures and sidewall heat flux conditions. The numerical simulations were conducted using ANSYS-Fluent. The studies have shown that different thermal environments can be created inside the enclosure, and cooling can be achieved with sufficient air exchange through vent holes. The instabilities due to buoyancy-driven flow are found to be necessary for air exchange through vent holes. Validation studies have shown that the heat flux from the sidewall should be considered, even if it is an excellent thermal insulator.

Article History

Received April 3, 2024
Revised June 25, 2024
Accepted August 3, 2024
Available online November 6, 2024

Keywords:

Thermal zone
Heat Sink
Ventilated Enclosure
CFD Analysis
Air Exchange

1. INTRODUCTION

Due to the increasing use of fertilizers, the grown plants are becoming poisonous. The popularity of home gardening has also increased in recent years. It is therefore necessary to produce vegetables that grow in different temperatures. By engaging in home gardening, individuals actively promote sustainability and biodiversity. Additionally, they significantly reduce carbon footprints by opting for locally grown food and adopting organic practices, ultimately leading to a healthier planet.

On the other hand, agricultural researchers conduct experiments and grow different cultivars in specialized laboratories. These cultivars often require specific environmental conditions. For small-scale cultivation, only a small area which meets the necessary parameters may be needed. Consequently, this controlled environment for cultivation can be achieved with small trays, containers, or enclosures. Control Environment Agriculture (CEA) was introduced to cultivate commercial crops within conditioned rooms or greenhouses. CEA recommends using heating, ventilation, and air conditioning (HVAC) to maintain the desired thermal environment for indoor farming. Maintaining a controlled environment throughout an entire room to facilitate this type of small-scale cultivation is expensive due to the high energy consumption associated with such practices.

The estimation of specific energy (kWh/kg crop) in CEA is influenced by environmental factors (Engler & Krarti, 2021), such as temperature, photosynthetically active radiation (PAR), and indoor CO_2 levels. In precision agriculture, it is not advisable to prioritize controlling power consumption by disregarding yield quality (Weidner et al., 2021). HVAC systems in cold storage for agricultural production function similarly to those used in CEA facilities. Both systems create and maintain a specific thermal environment to prevent spoilage of stored goods. Energy consumption increases linearly as per the increase in the volume of cold storage (Evans et al., 2014). Ventilation is not an option for temperature control if the ambient temperature differs considerably from the desired temperature. Ventilation mainly promotes fresh air interaction and CO_2 level minimization within the plant factory. Revathi et al. (2019) estimated 1.48 kWh of energy consumption from

NOMENCLATURE

C_p	specific heat capacity of the fluid	T	temperature of the fluid
g	acceleration due to gravity	T_{air}	temperature of the air
k	thermal conductivity of the fluid	T_{sink}	heat sink temperature
k	turbulent kinetic energy	S	source term
$u, v, and\ w$	velocities components in the x, y, and z directions respectively	μ	dynamic viscosity
U	average velocity of the fluid	ε	rate of dissipation of turbulent kinetic energy
p	fluid pressure	ρ	density of the fluid
t	time	Gr	Grashof Number
Ra	Rayleigh Number	Pr	Prandtl Number

using four ventilation fans in the greenhouse. High energy consumption is the primary factor affecting CEA's environmental sustainability concerns. The energy consumption in the CEA mainly depends on the external environment (Weidner et al., 2021). Pasapuleti et al. (2022) delve primarily into sustainable agriculture in transport containers, focusing on net-zero energy. The case study involved ten mushroom farming transport containers, each with a volume of 72.60 cu. m. The estimated specific energy consumption per hour per container was 8.793 kW. In a recent study by (Sheikholeslami & Khalili, 2024b), a new heat transfer tube was incorporated into the photovoltaic thermal cooling system. Furthermore, Sheikholeslami & Khalili, (2024b) conducted an energy analysis on a similar system that utilized nanofluid through the heat transfer tube. Dimova et al. (2020) successfully developed the energy-efficient "Kaldnitsa" mushroom production plant in Stara Zagora, Bulgaria. The plant implemented a groundwater evaporative cooling system for air conditioning in mushroom production. Nonetheless, the total specific energy consumption depends upon the crop growth stages. The HVAC system needs to be designed based on the high demand for specific energy consumption. Determining the heating, ventilation, and air conditioning (HVAC) design for a particular crop cultivation room is contingent upon the computations of the cooling load. These calculations are derived from various factors, including the desired cooling conditions of the crop, the thermal influence from external sources, the utilization of LED systems for photosynthesis, the thermal capacity of the materials and furniture employed in the construction, the room's ventilation, and the presence of individuals working within the space (Ashrae, 2021). In contrast to compact enclosure crop cultivation, this assessment considers only a few specific factors, such as the required cooling conditions with humidity, reduced air circulation, and limited input from LED sources. Using less cooling energy for small-scale indoor crop production can save electricity used by HVAC systems. This approach creates multiple thermal zones (TZ) within a single room, as illustrated in Fig. 1. Multiple thermal zones can be established in a single room using small enclosures with adiabatic walls.

Eco-friendly Peltier cooling systems are more convenient for cooling small-scale enclosures than vapour compression refrigeration (VCR) or vapour absorption refrigeration systems. Peltier coolers mainly work on the Peltier effect principle. The Peltier effect creates a temperature difference at the junctions of two dissimilar semiconductors through the application of electric current across the junction (Daimon et al., 2016; Ibikunle et al., 2022). Though the Peltier is less efficient, using it in the enclosures is convenient to make them as multiple thermal zones (TZs). Rudresha et al. (2023) used computational fluid dynamics (CFD) to examine three distinct thermo-electric refrigerators (TER) models with insulating materials. Previous studies have shown that the location and orientation of the Peltier heat sink inside an enclosed space have a strong influence on the cooling characteristics (Söylemez et al., 2019). Studies have shown that uniform cooling can be achievable using a Thermoelectric cooler (TEC) (Söylemez et al., 2021). A comparison study was carried out by Afshari (2021) between air-to-air and air-to-water heat exchangers to determine the TEC refrigerator's cooling efficacy. The air-to-air TEC refrigerator enclosure maintains an average air temperature (T_{air}) of up to 16°C. The TEC refrigerator with hot side heat exchanger heat dissipation was examined by Afshari et al. (2023). The average air temperature was maintained up to 15°C inside the enclosure using a single Peltier (TEC-12715). Astrain et al. (2005) developed the computational model and carried out the experimental thermal analysis of the TEC refrigerator. All studies on the prototype revealed that the refrigerator's interior temperature is proportional to the ambient temperature. The interior temperature of 13°C was maintained when the ambient temperature was 32°C.

Researchers have expressed considerable interest in investigating natural convection within enclosures. This flow, prompted by buoyancy, gives rise to instabilities within the enclosure, significantly influencing heat transfer. Characterizing buoyancy-driven flow involves using dimensionless numbers such as Grashof (Gr) or Rayleigh (Ra). Wen et al. (2021) numerically studied the air-filled square cavity to understand the nonuniform density variation due to large temperature fluctuations. This leads to instability-driven flow within the cavity. Instability occurs when the orientation of the inlet changes for horizontal liquid-liquid flow (Morgan et al., 2017). Singh & Singh (2019) investigated the natural convection heat transfer of a micropolar fluid flow between two vertical concentric cylinders using the Boussinesq approximation. Bouras et al., (2021) conducted a numerical investigation of a cubical enclosure using the standard k-ε turbulence model. With a Gr of 10^9, this identified the buoyancy-driven flow within the enclosure. Kumar & Subudhi (2020) examined a water-filled cubic

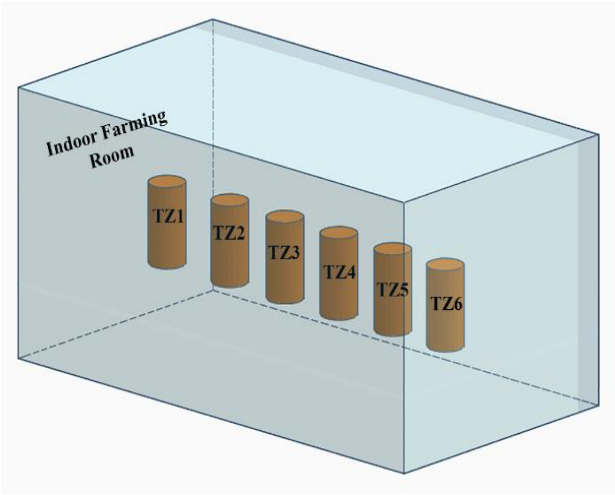

Fig. 1 Conceptual picture of an indoor farming room with numbers of different thermal zone enclosures

cavity heated from below and opened at the top. The main findings show that Rayleigh number of 10^5–10^9 and Prandtl Number (Pr) of 4-6 cause turbulent convection. Iyi et al. (2018) conducted a numerical and experimental natural convection study for low turbulence flow in an air-filled enclosure with cylindrical obstructions. Heat transfer within the enclosure results in a Rayleigh number of 4.04 x 10^9. Plourabouéet al. (2024) used the Boussinesq approximation and the Gr between $7x10^3$ and $5x10^6$ to look at the natural convective loop numerically and theoretically. Bhattacharya and Das, (2015) used the Boussinesq approximation with the Ra (10^3–10^7) to examine the buoyancy-driven flow inside the square cavity numerically. Results show that fluid particles become unstable as the Ra increases, and increased velocity results in better heat transfer.

Culturing various crops in distinct thermal environments, such as Cole crops and mushrooms, is a promising prospect. A proposed system has the potential to support the cultivation of these crops within a single enclosed space. For example, optimal vegetative growth for cauliflower occurs within a temperature range of 15°C to 22°C, with growth ceasing above 30°C. Fluctuating temperatures may lead certain cauliflower cultivars to revert to vegetative growth, resulting in suboptimal bract formation (Fordham & Hadley, 2003; Rubatzky & Yamaguchi, 2012). Consequently, with the appropriate micro- and macronutrients; Cole crops are well-suited for small-scale production. Conversely, mushrooms are highly sought after due to their abundant nutritional content. It is important to note that various types of mushrooms, including medicinal varieties and button mushrooms, require specific temperature conditions at different growth stages. For instance, button mushrooms flourish at an air temperature of 14–18°C during the fruiting stage (Khan & Chandra, 2017; Netam et al., 2018). Many organic farmers are interested in these crops due to their adaptability, health benefits, compatibility with planting rotations, and pest-suppressive properties. The economic feasibility of Cole crop cultivation can vary significantly based on the specific crop and the geographic region. Smaller producers can reach customers directly through farmer's markets and roadside stalls. Therefore, the proposed idea of focusing on small-scale cultivation of different crops in a single room can be beneficial.

The authors intend to investigate a simple, convenient, and affordable enclosure that can be used to create multiple TZ's in a single room. A TZ can be cold; another can be warm. A TZ may have a higher air exchange rate, another low, etc. Every specific enclosure used in the room can be customized to have a particular TZ. In the present paper, the authors propose a cylindrical ventilated enclosure in which the two Peltier surfaces are used as heat sinks for cold dissipation. A CFD tool was used to carry out various simulation experiments to study the influence of heat sink temperatures, ventilation, orientation of the heat sink, and heat flux from cylinder wall material on the enclosure temperature. Since 15°C – 25°C was the ideal temperature range for the proper growth of the vegetables (Lakhiar et al., 2018), the objective of the present work was to achieve a T_{air} in the cylindrical enclosure of less than 25°C, while the T_{air} at the inlet and outlet openings was around 37°C, referred to as the surrounding room temperature in warm climatic regions during summer.

2. EXPERIMENTAL SETUP AND NUMERICAL GEOMETRY DETAILS

A closed cylindrical enclosure was constructed using a Mild steel mesh to maintain the cylindrical shape of the Styrofoam insulation with minimal thermal mass. The dimensions of the cylinder were 0.5 meters in diameter and 0.6 meters in height. The insulation included a 25mm thick layer of Styrofoam with a thermal conductivity ranging from 0.025-0.03 W/m-K. Two Peltier cooler assemblies, along with TEC1-12706 Peltier modules, were positioned near the top of the cylindrical enclosure, as represented in Fig. 2. Additionally, a 2W DC cooling fan was coupled with the cold surface of the Peltier modules, while a 5W DC cooling fan was integrated with the hot surface to ensure effective convective cooling and eliminate any impact on the thermal environment of the enclosure. Thermocouples were strategically placed inside the enclosure for temperature measurements at different heights and recorded using a data acquisition system (DAQ).

2.1 Numerical Geometry Details

Two similar enclosure configurations with different orientations of the heat sinks were considered in the present simulations, as shown in Fig. 3. The enclosure dimensions used in the CFD simulations were the same as those used in the physical experiments, as shown in Fig 2. The enclosure was 0.5m in diameter and 0.6m in height. The model had four vents (40mm in diameter) on the top and bottom surfaces of the enclosure. The vent holes were provided as the crops needed air exchange. In both the configurations and the physical experiments, the Peltier heat sinks were located near the sidewall (around 30mm) and the enclosure's top surface (around 100mm). The size of the Peltier heat sinks was 60mmx60mm. The two configurations were different regarding the orientation of

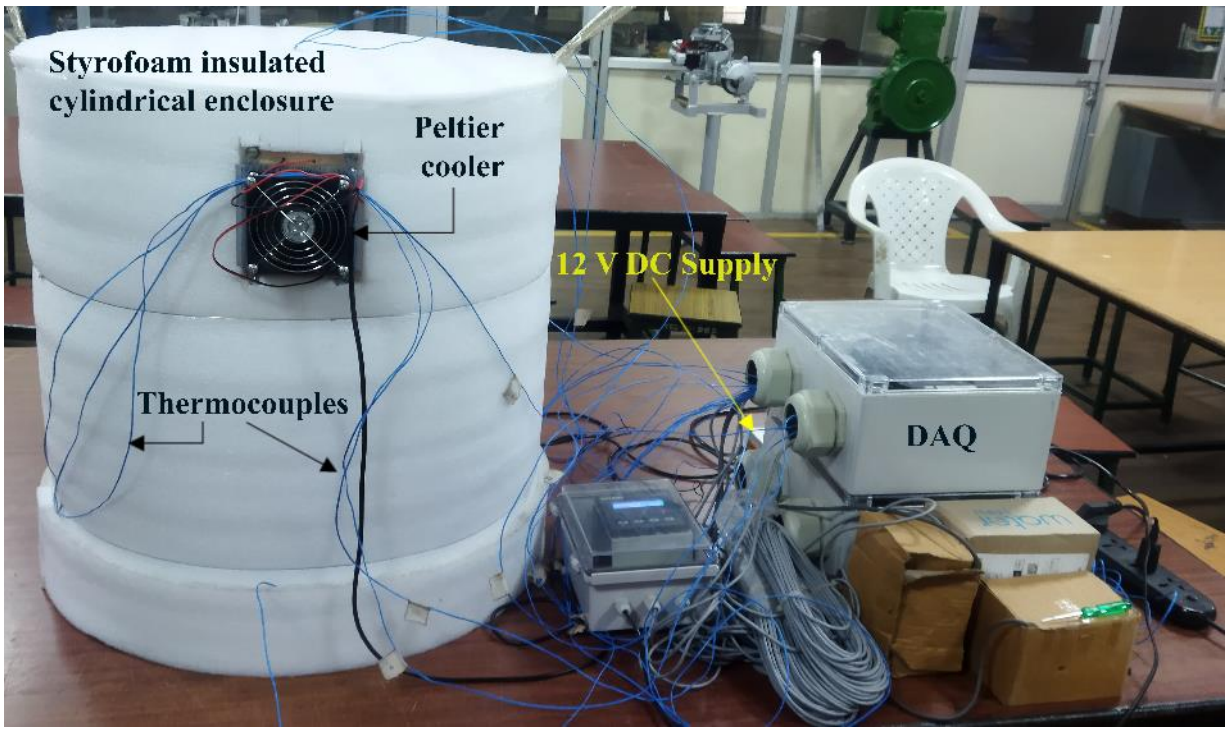

Fig. 2 Enclosure air cooling experimental setup

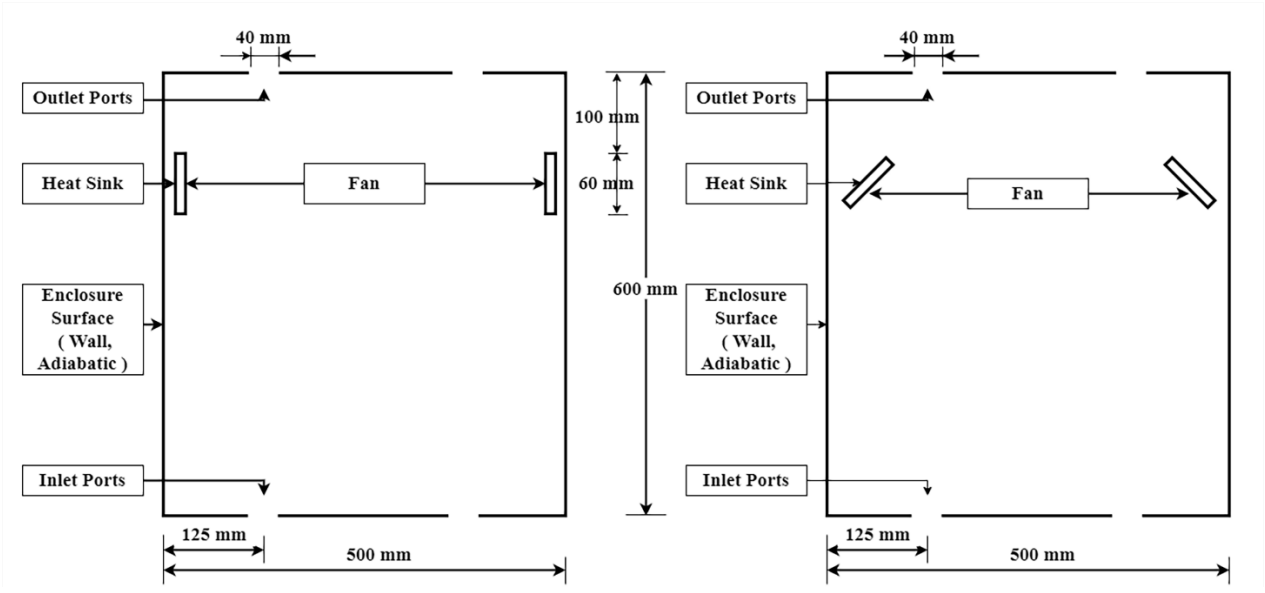

(a) (b)

Fig. 3 Schematic representation of the geometry configurations (a) Case 1- a cylindrical ventilated enclosure with two square vertical heat sinks with fans (b) Case 2- a cylindrical ventilated enclosure with two inward 45° inclined square heat sinks with fans

the Peltier heat sinks. As per the surface area of the fan used in the physical experiments, fan boundary conditions with suitable surface area were applied. The hot surface of the Peltier was not considered in the present simulations as it was external to the enclosure domain. The use of such low energy-consuming fans can make the system affordable.

The rationale behind selecting the orientations mentioned above lies in defining the Gr. Higher Gr values indicate the presence of higher buoyancy forces in the natural convective flows. These buoyancy forces could help in air exchange. Gr can be increased by increasing the temperature difference or changing the inclination. Other parameters can also affect the Gr. Changing the orientation is cost-effective compared to raising the temperature difference in the present problem. The main objective was to study the thermal diffusion inside the enclosure while allowing some air to exchange through the vent holes of the enclosure. Hence, the authors intended to study two different orientations of heat sinks.

Table 1 Mesh quality

Parameter	Configuration 1	Configuration 2	Reference Value	Result
Element quality	0.8429	0.84363	0-1	Optimal
Aspect ratio	1.8213	1.8178	1-∞	High quality
Skewness	0.22329	0.22228	0-1	Excellent
Orthogonal Quality	0.77299	0.7741	0-1	Good

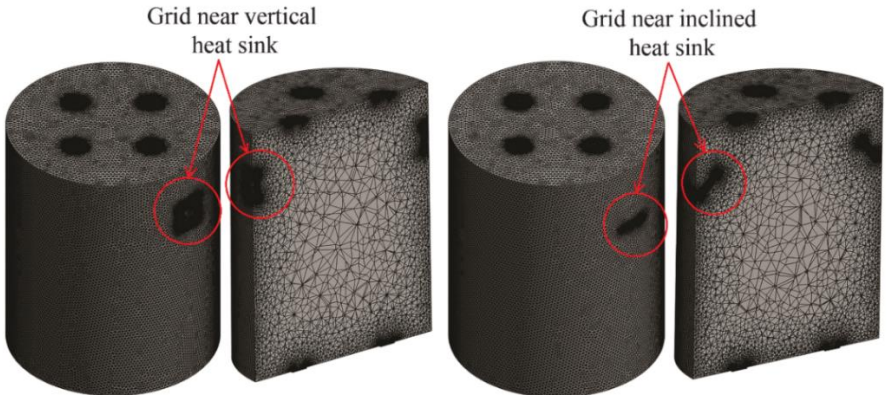

(a) (b)

Fig. 4 Computational meshing of cylindrical ventilated enclosure geometry models a) vertically oriented heat sinks with sectional view, and b) 45º inclined heat sinks with sectional view

Table 2 Grid Independence study

Mesh Elements	Enclosure Volume Average Temperature (°C)
611984	37.54
763133	36.19
1246738	34.11
1413532	33.58
1559506	33.48

2.2 Meshing and Grid Independence Study

Grid generation was carried out using Ansys 2022 R2 Meshing software. It consists of unstructured meshing with maximum tetrahedron mesh elements. Mesh quality was checked for the Element quality, Aspect ratio, Skewness, and Orthogonal quality per the referral values in Table 1. Several studies have validated the use of unstructured grids in such thermal diffusion convection problems (Söylemez et al., 2019; Afshari, 2021; Söylemez et al., 2021).

Figure 4 shows the computational meshing of cylindrical ventilated enclosure geometry models: a) vertically oriented heat sink and b) 45° inclined heat sinks. Figure 4 also indicates the sectional views for the case with unstructured mesh and grid arrangements near the vertical and inclined heat sinks.

The simulated results were verified to be grid-independent. Five different mesh qualities were used in the grid independence studies, as tabulated in Table 2. A variation in the volume average temperature of the enclosure was observed to change by less than 1% with 1413532 elements. One of the configurations was tested, and the corresponding grid quality was used in all the simulations.

3. GOVERNING EQUATIONS, ASSUMPTIONS, AND BOUNDARY CONDITIONS

ANSYS Fluent Flow 3D simulation software was used to solve the equations that govern fluid flow. The solution domain was divided into smaller control volumes and analyzed. The Reynolds Average Navier-Stokes (RANS) equations were solved simultaneously using a second-order implicit transient state approach and a standard k-ε turbulence model. A similar approach is reported in the literature (Afshari, 2021).

3.1 Assumptions Involved

The following assumptions are involved in the present simulations:

1. Air is an incompressible fluid with constant properties.
2. Air is a Newtonian fluid
3. Boussinesq approximation holds well in the present mixed convection airflow conditions.
4. Radiation effects are negligible between the heat sinks, enclosure walls, and the air.

3.2 Governing Equations

The RANS equations were used to solve the flow in the simulations.

1. Conservation of mass equation (Continuity equation)

Incompressible flow conservation of mass equation Eq. (1)

$$\frac{\partial \rho}{\partial t} + \text{div}(\rho \boldsymbol{U}) = 0 \tag{1}$$

2. Conservation of momentum

Incompressible flow Newtonian fluid conservation of momentum equations (RANS) Eq. (2-4)

$$\frac{\partial(\rho \boldsymbol{u})}{\partial t} + div(\rho \boldsymbol{u}\boldsymbol{U}) = \left(-\frac{\partial p}{\partial x}\right) + \mu\, div(grad\, \boldsymbol{u}) + \left[-\frac{\partial\left(\rho \overline{\boldsymbol{u'^2}}\right)}{\partial x} - \frac{\partial(\rho \overline{\boldsymbol{u'v'}})}{\partial y} - \frac{\partial(\rho \overline{\boldsymbol{u'w'}})}{\partial z}\right] + \boldsymbol{Su} \tag{2}$$

$$\frac{\partial(\rho \boldsymbol{v})}{\partial t} + div(\rho \boldsymbol{v}\boldsymbol{U}) = \left(-\frac{\partial p}{\partial y}\right) + \mu\, div(grad\, \boldsymbol{v}) + \left[-\frac{\partial(\rho \overline{\boldsymbol{u'v'}})}{\partial x} - \frac{\partial\left(\rho \overline{\boldsymbol{v'^2}}\right)}{\partial y} - \frac{\partial(\rho \overline{\boldsymbol{v'w'}})}{\partial z}\right] + \boldsymbol{Sv} \tag{3}$$

$$\frac{\partial(\rho \boldsymbol{w})}{\partial t} + div(\rho \boldsymbol{w}\boldsymbol{U}) = \left(-\frac{\partial p}{\partial z}\right) + \mu\, div(grad\, \boldsymbol{w}) + \left[-\frac{\partial(\rho \overline{\boldsymbol{u'w'}})}{\partial x} - \frac{\partial(\rho \overline{\boldsymbol{v'w'}})}{\partial y} - \frac{\partial\left(\rho \overline{\boldsymbol{w'^2}}\right)}{\partial z}\right] + \boldsymbol{Sw} \tag{4}$$

Here, S represents the source terms with values

$$\boldsymbol{Su} = \boldsymbol{Sw} = 0, and\ \boldsymbol{Sv} = -\rho g$$

3. Conservation of energy

The first law of Thermodynamics for the incompressible fluid is given by in Eq. (5),

$$\frac{\partial(\rho \boldsymbol{T})}{\partial t} + div(\rho \boldsymbol{U}\boldsymbol{T}) = div\left(\frac{k}{C_p} grad\, \boldsymbol{T}\right) + \left[-\frac{\partial(\rho \overline{\boldsymbol{u'T'}})}{\partial x} - \frac{\partial(\rho \overline{\boldsymbol{v'T'}})}{\partial y} - \frac{\partial(\rho \overline{\boldsymbol{w'T'}})}{\partial z}\right] + \boldsymbol{S} \tag{5}$$

Here $\boldsymbol{S} = \boldsymbol{0}$ is assumed for the adiabatic wall and the value of $\boldsymbol{S}$ may change according to heat flux from the wall.

3.3 Boundary Conditions

The details of various boundary conditions applied to the components of the enclosure are tabulated in Table 3. Two different cases with three different temperature values of the Peltier cold surface 12°C, 6°C, and 0°C were analyzed through simulations. Overall, 12 cases were analyzed in the present work and the same are tabulated in Table 4.

3.4 Simulation Settings, Convergence Criteria

Numerical simulations were conducted using Fluent Flow Software (ANSYS 2022 R2) and a hardware system with a 12th Gen Intel® Core™ i9-12900K 3.20 GHz processor and 64 GB of RAM. The Coupled scheme was used for pressure-velocity coupling during the simulation. The second-order discretization method was used to calculate pressure values, and the second-order upwind scheme was used to solve momentum and energy equations; on the other hand, the first-order upwind scheme was used for turbulent kinetic energy and turbulent kinetic energy dissipation rate in standard k-ε turbulence model. Similarly, a Coupled scheme and the standard k-ε were used by Afshari et al. (2023) in the CFD simulations. A standard k-ε model was used to simulate all three models of the TER system (Rudresha et al., 2023). The simulation results with standard k-ε, realizable k-ε, and transition SST turbulence showed no significant

Table 3 Boundary conditions applied at the various components of the geometry

Sr. No.	Component	Conditions	Value
1	Bottom Surface Ports	Inlet Vent	1 Atmospheric, 37°C
2	Top surface Ports	Outlet Vent	1 Atmospheric, 37°C
3	Heat sinks	Wall	i) 0°C ii) 6°C iii) 12°C
4	Fan	Fan	5 Pa
5	Cylindrical enclosure	Wall	i) Adiabatic ii) 8 W/m^2

Table 4 Identification of the configuration based on the boundary conditions and heat sink orientation

Case Name	Heat Sink Orientation	Heat Sink Temperature Boundary Condition	Enclosure Wall Heat Flux Boundary Condition
Case1-T12-q0	Vertical	12°C	Adiabatic
Case 1-T12-q8			8 W/m^2
Case 1-T6-q0		6°C	Adiabatic
Case 1-T6-q8			8 W/m^2
Case 1-T0-q0		0°C	Adiabatic
Case 1-T6-q8			8 W/m^2
Case 2-T12-q0	45° Inclined	12°C	Adiabatic
Case 2-T12-q8			8 W/m^2
Case 2-T6-q0		6°C	Adiabatic
Case 2-T6-q8			8 W/m^2
Case 2-T0-q0		0°C	Adiabatic
Case 2-T0-q8			8 W/m^2

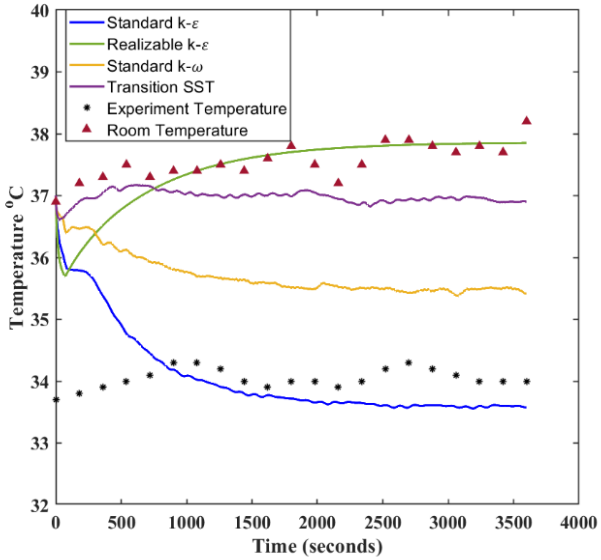

Fig. 5 Validation of the CFD simulated temperature to an experimentally observed temperature

differences (Söylemez et al., 2021). Convergence criteria of 10^{-3} were used for continuity, momentum, and turbulence equations, and 10^{-6} for the energy equation. 5% turbulence intensity at the inlet and outlet openings was set in all the simulations. The above-mentioned basic simulation settings were used in all the simulations.

4. Results and Discussion

The study has been conducted to thoroughly examine twelve suggested configurations outlined in Table 4, which included vertical and inclined heat sink orientations and three potential heat sink temperatures: 12°C, 6°C, and 0°C. The key parameters of this study are the air temperature within the enclosure, velocity, and Gr. Among the twelve configurations, case 2 is particularly significant for comprehending the impact of inclination on the mixing and diffusion of cold air within the enclosure. The selected configurations are cost-effective and user-friendly. This section provides a detailed analysis of the enclosure air parameters.

4.1 Numerical Simulation Validation

In this study, CFD simulation results were compared with the temperature outcomes from the fabricated experimental setup, as shown in Fig. 2. The average temperature of the enclosure air in case 1 was used to validate the simulated temperature without inlet-outlet vents. Based on the Peltier cold surface measured temperature, the temperature boundary condition was applied for the heat sink surfaces in the numerical study. This validation compares simulation results of Standard k-ε, Realizable k-ε, Standard k-ω, and Transition SST turbulence models with experimental results. The standard k-ε model accurately predicts the enclosure's average volume temperature, shown in Fig. 5. Airflow inside the enclosure has minimal interaction with solid boundaries, promoting the validated results with the standard k-ε turbulence model. The enclosure's airflow ensures low Reynolds number flow; therefore, the standard k-ε was well suited for the current CFD simulation. Standard k-ε is a widely used, well-established, robust, and simple turbulence model. It requires fewer computational resources compared with other complex models. It is relatively easy to implement. Compared to other turbulence models, the current CFD simulation studies for the enclosure use the standard k-ε in minimal time (Bouras et al., 2021). Realizable k-ε is an improved version of the standard model, but it is unable to capture the flow conditions within the enclosure after 100s. Standard k- ω is more sensitive to mesh quality and boundary conditions, potentially leading to less accurate results in the current study. The main design of Transition SST was to handle transitional flows from laminar to turbulent, which may differ from the dominant flow regime in the current study of low Reynolds number flow within the enclosure. Furthermore, all the simulations used the standard k-ε turbulence model.

Simulations were conducted for 60 minutes of physical time, using a time step of 1 second. All the simulations considered the room temperature as constant at 37ºC. Hence, the standard k-ε turbulence model predicted temperature reduces during the 0-1000s and maintains the steady temperature within the enclosure. However, the experiment started well before and ran for a few hours, and a steady temperature within the enclosure was observed. During the experimentation, the room temperature was varied from 30°C in the morning to a maximum of 37°C in the afternoon. A steady state situation from the experiments was selected for the validation, i.e. when the room temperature was around 37°C for more than 60 minutes. The average enclosure T_{air} was around 34°C during this period, as shown in Fig. 5. The results of the simulated standard k-ε turbulence model and the measured temperatures showed good agreement. The temperature difference was found to be no more than 0.6°C. Furthermore, all the simulations used similar boundary conditions, solver settings, and convergence criteria.

4.2 Influence of Sidewall Insulation on Enclosure Air Temperature

As previously mentioned, temperature significantly influences plant growth at all stages. To prevent heat transfer from the surrounding environment, it is crucial to insulate the enclosure effectively. Styrofoam was chosen as the sidewall insulation material due to its widespread availability and ease of use. However, it is important to acknowledge that no real material is a perfect insulator. In this context, Peltier devices are proposed as heat sinks to minimize electricity consumption. Efficient cooling of the enclosure requires consideration of heat transfer through the sidewall despite its insulating properties. Experimental results indicate that heat transfer through the sidewall is 8 W/m² under steady-state conditions. Additionally, simulations were conducted under adiabatic wall conditions to examine the role of heat transfer through the sidewall. All the numerical simulations were started with an initial guess of enclosure temperature of 37°C, assuming it to be the same as the surrounding air temperature. The exact value was also considered at inlet

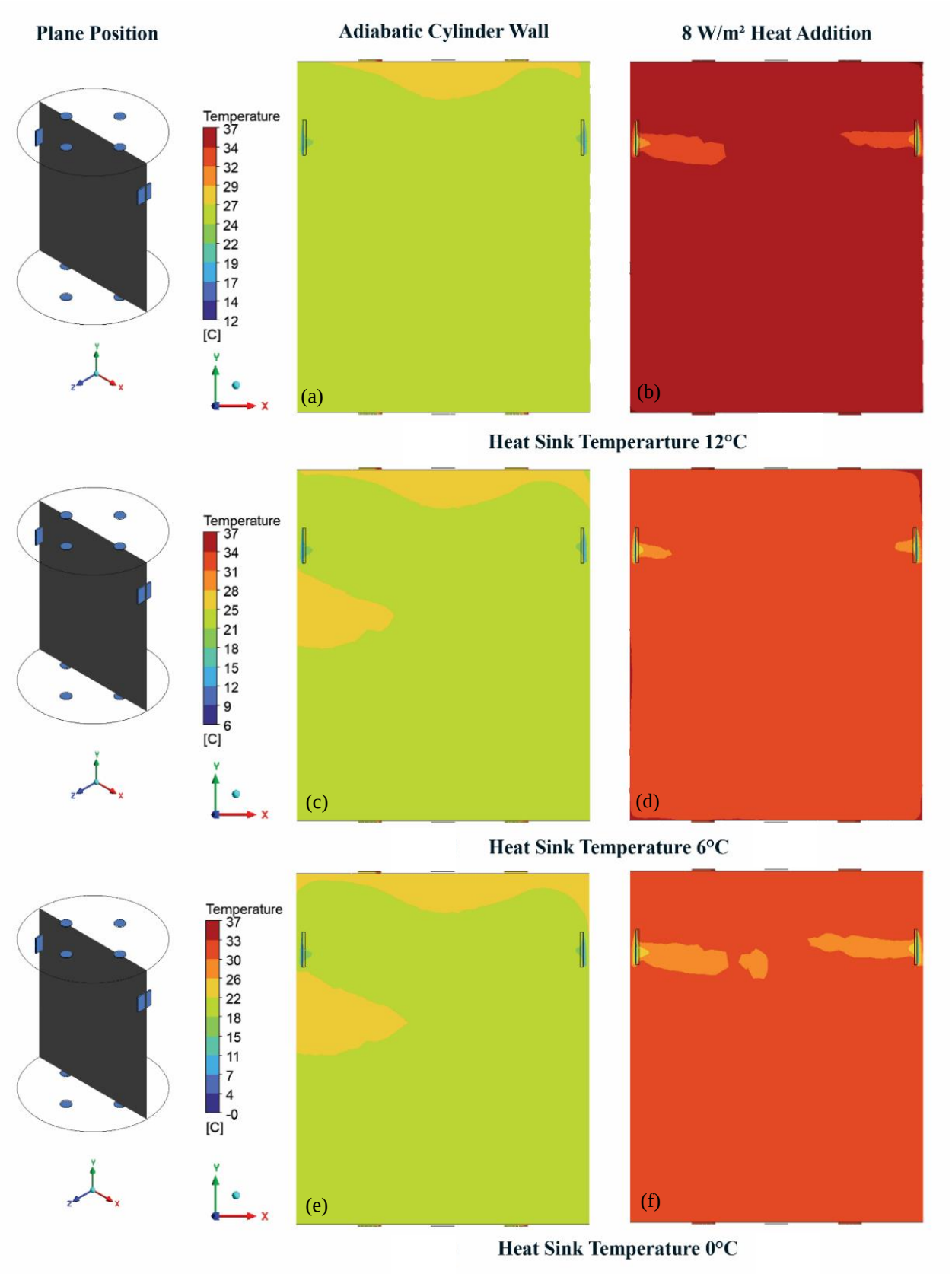

Fig. 6 Temperature contours of the case 1 vertical heat sink

and outlet ports since it was the opening for the air exchange.

Temperature contours for case 1 vertical orientation heat sink geometrical model simulation experiments are presented in Fig. 6. The results for Case1-T12-q0 and Case1-T12-q8 are shown in Fig. 6 a and b. As observed in Fig. 6 (b), isotherms show that cooling can have a considerable influence due to the cold surfaces up to around 0.125m to 0.2m horizontally in opposite

directions. A T_{air} reduction of 29–32°C was observed in this region. The remaining entire enclosure air had negligible influence on the presence of heat sink surfaces. The average entire enclosure temperature reached 34°C.On the other hand, with similar heat sink conditions, perfectly insulated cylinder walls show sound temperature reduction in the enclosure. Figure 6 (a) demonstrates the temperature variation in the enclosure for Case1-T12-q0 with an adiabatic cylinder wall. Compared to the heat addition condition, an adiabatic wall showed better thermal diffusion in the enclosure with a temperature of up to 24°C. The effect of 37°C inflow air from the upper vents was detected in the air at the central top portion surrounding the vent holes of the enclosure. This portion reached a T_{air} of 27–29°C.

For Case1-T6-q0 and Case1-T6-q8 as the T_{sink} =6°C, the temperature contours are detailed in Fig. 6 c and d. Most of the enclosure air was observed to have uniform temperature even when the heat flux of 8W/m^2 (Fig. 6 d) from the sidewall and obviously for adiabatic wall condition (Fig. 6 c). The average enclosure T_{air} with and without heat flux from the sidewall was 31°C and 21°C, respectively. The observations were similar for Case1-T0-q0 and Case1-T0-q8 if the T_{sink}=0°C. However, in the latter case, the average enclosure T_{air} with and without heat flux from the wall was 30°C and 18°C, respectively, as depicted in Fig. 6 e and f. Similar temperature contours were obtained with Case 2 as the heat sink inclined at 45^o, as shown in Fig. 7 a – f. For Case 2-T12-q0 and Case 2-T12-q8 of T_{sink} = 12°C with sidewall heat flux (Fig. 7 b), no significant difference in T_{air} was observed compared to that of without inclination (Fig. 6-b). But the same without heat flux from the sidewall (Fig. 7-a) was found to reach a relatively higher temperature inside the enclosure (27 – 29°C) as compared to the vertical sink case shown in Fig. 6-a (24 – 27°C).

A similar analysis was carried out for T_{sink} = 6°C (Case 2-T6-q0 and Case 2-T6-q8) and T_{sink} = 0°C (Case 2-T0-q0 and Case 2-T0-q8) cases with heat sink inclined at 45^o. The temperature contour plots for the same are shown in Fig.7 c-f. The T_{air} was observed to remain higher (25 – 28°C) if the heat sinks were inclined facing down without heat flux from the sidewall, while the same was around 21– 25°C if the heat sinks were oriented vertically. However, when the heat flux from the sidewall is considered, there is not much difference in the temperature fields except near the wall. Similar observations were made when the T_{sink} was set to 0°C. The temperature contours are abortive to determine the influence of the difference between T_{air} inside the enclosure and the surrounding T_{air} on the air exchange rate. Hence, it is essential to investigate the streamline contours and vector plots.

4.3 Influence of Convection and Diffusion on Air Exchange Through Vents

Understanding the influence of convection and diffusion within the enclosure on the air exchange rate through the vents is a significant step in the field of fluid dynamics and ventilation systems. This understanding is facilitated by the analysis of the velocity vector plots and streamline contours, as shown in Fig. 8, 9, 10, and 11. The magnitude of the air velocity at the exit of the modelled fan surface is notably influenced by the inclination, regardless of the sidewall heat flux, further contributing to our knowledge in this area.

Figure 8 and 9 depict the vector plots and streamlined contours of the cases with the heat sink oriented vertically. From Fig. 8 a–f, the velocity vectors for all conditions of case 1 are identical; even the streamline contours from Fig. 9 a–l showed no significant difference. The maximum velocity of air due to the fans with a 5Pa pressure difference, which consumes 2W power, was found to be 2.32 m/s, which is shown in Fig. 8. Though the cold air streams of the same temperature exit the fans placed opposite to each other, one of them gets pushed towards the top of the enclosure against the gravity force. This can be due to two reasons: (i) Low-pressure recirculation zones get created around both fans due to mass entrainment, and (b) the air particles of both streams exchange momentum at a distance equal to both fans. One of the air streams reaches the top surface vent holes, and the other goes to the bottom surface vent holes. Hence, fans with a 5Pa pressure difference and heat sinks could create air exchange and cooling. This is an essential requirement in indoor farming. This is observed to be the same for all the cases with heat sinks/fans placed vertically. On the other hand, the streamlines shown in Fig. 9 hint at the fact that the residing time of the air below the plane of the fans is higher due to recirculation.

Two vents from the top face and two vent holes from the bottom face are involved in the air intake action, and the remaining vents are for the air outlet, as observed in Fig. 9 a-l. Streamlines also show the presence of still air in the lower core region, which is cooled by conduction. The study suggests this is the best location to place the compost/soil container. For all the case 1 simulations, an average airflow from the enclosure was observed to be constant of value 0.2×10^{-3} kg/s. This mass flow rate translates into 5 air exchanges per hour from the enclosure. Fig. 10 a–f depicts the velocity vector fields of case 2, i.e., with an inclined heat sink. A maximum air velocity of 2.45 m/s was observed immediately after the fans. All the case studies in Fig. 10 a–f showed similar velocity vector patterns for case 2. A negligible difference in the flow characteristics with and without heat flux from the sidewall was observed in the case of T_{sink} =12°C (Case 2-T12-q0 and Case 2-T12-q8) as inferred from Fig. 10-a, b, and 11-a-d. However, the flow characteristics change due to heat flux from the sidewall when the T_{sink} is set to 6°C and 0°C. The mixing enhances towards the bottom of the enclosure below the fan's plane as the heat sink surface temperature is reduced (Fig. 11-e-l). Unlike the case-1 vertical heat sink, where a region of still air was observed, a pointed air stream could be observed with the inclined heat sink. Hence, the latter configuration could be used for crops whose leaves need airflow, as seen in Fig. 11-b, d, f, h, j, and l. However, still air zones have been observed in case 2 of inclined heat sinks, particularly just above the region where the two air streams meet. This region can be used for plant hanger fixtures for compost placement. This is typically required for the hanging of mushroom bags. The average flow rate for the enclosure system in case 2 is

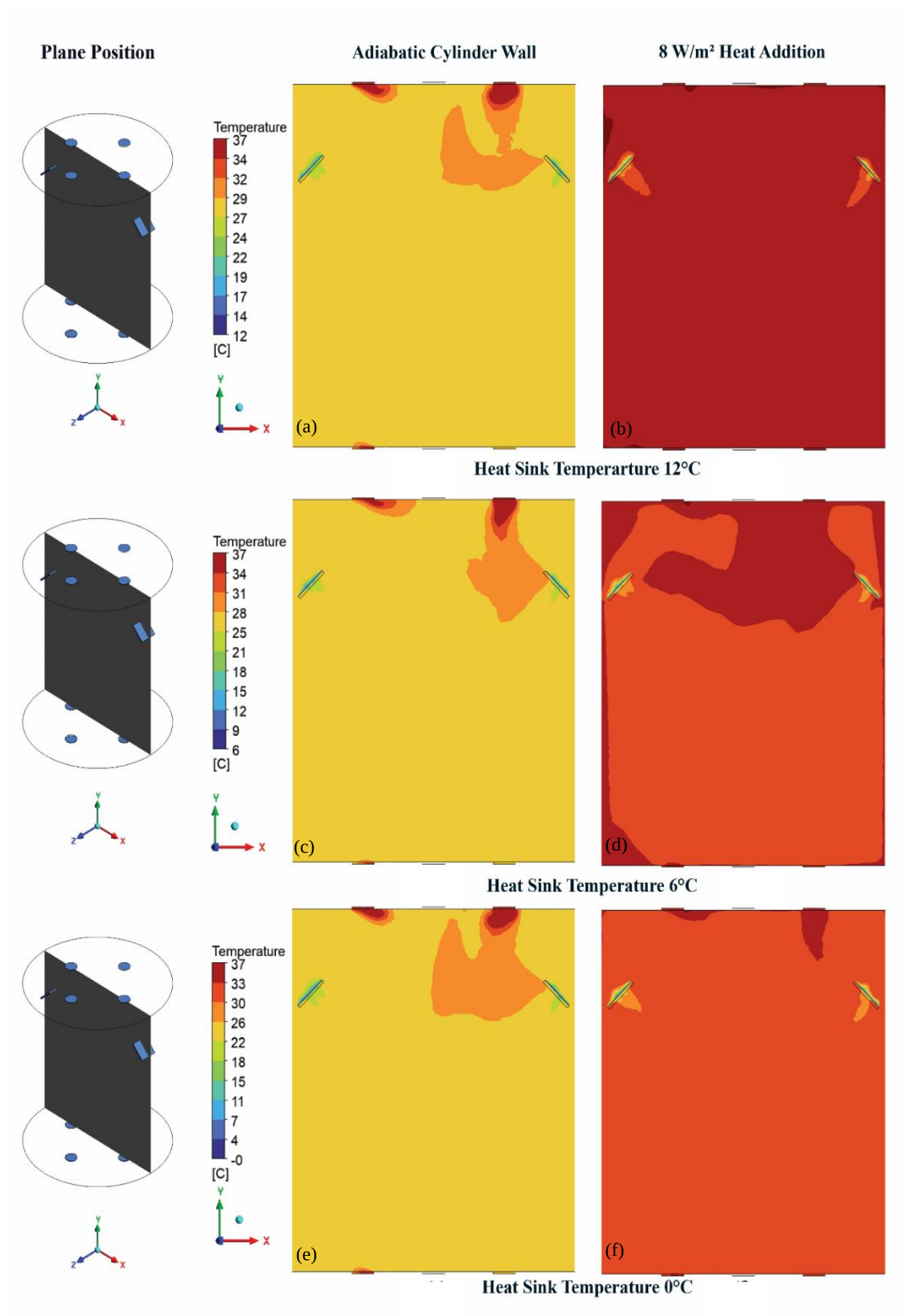

Fig. 7 Temperature contours of the case 2 inclined heat sink

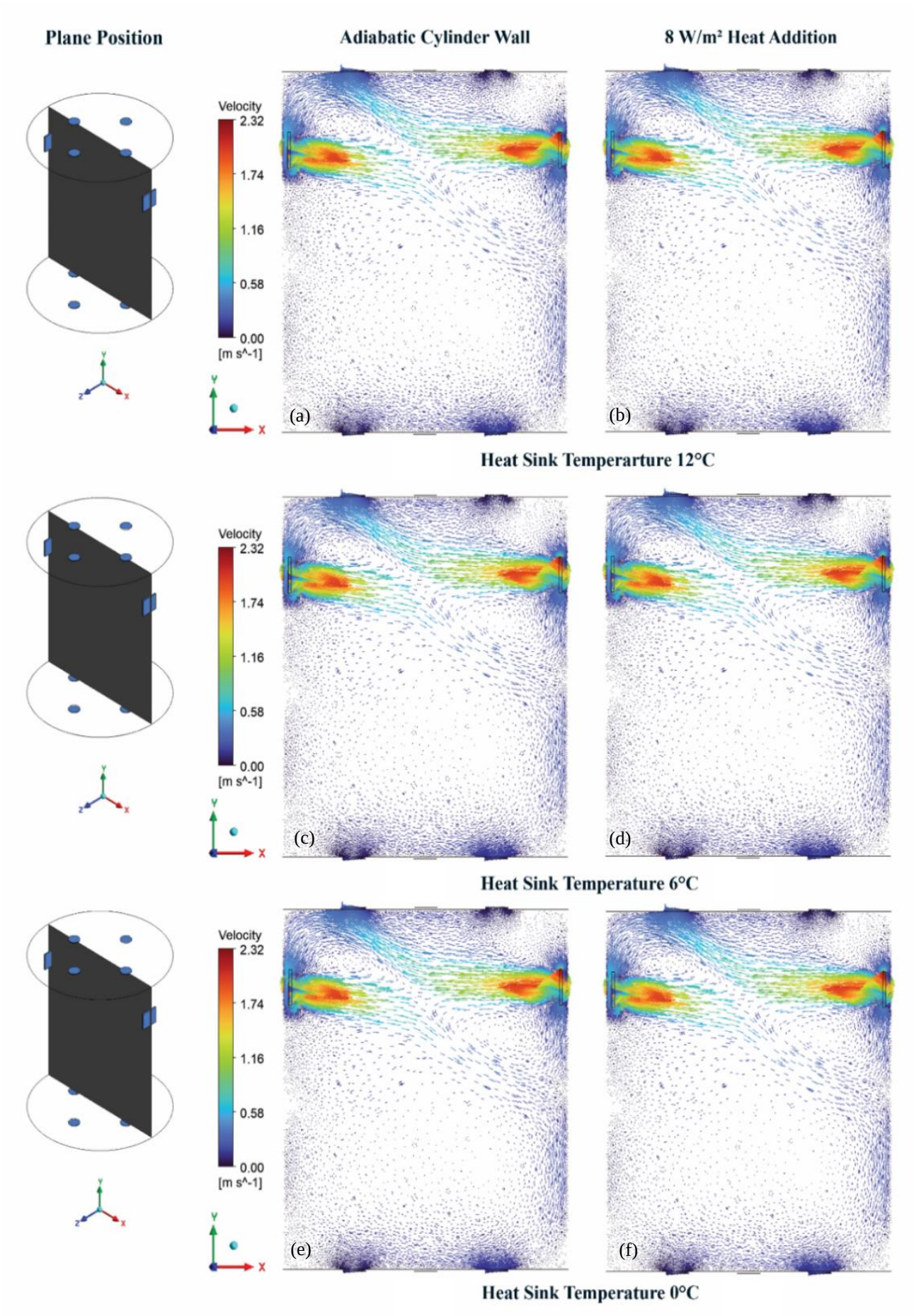

Fig. 8 Velocity vector plot of case 1 vertically oriented heat sink

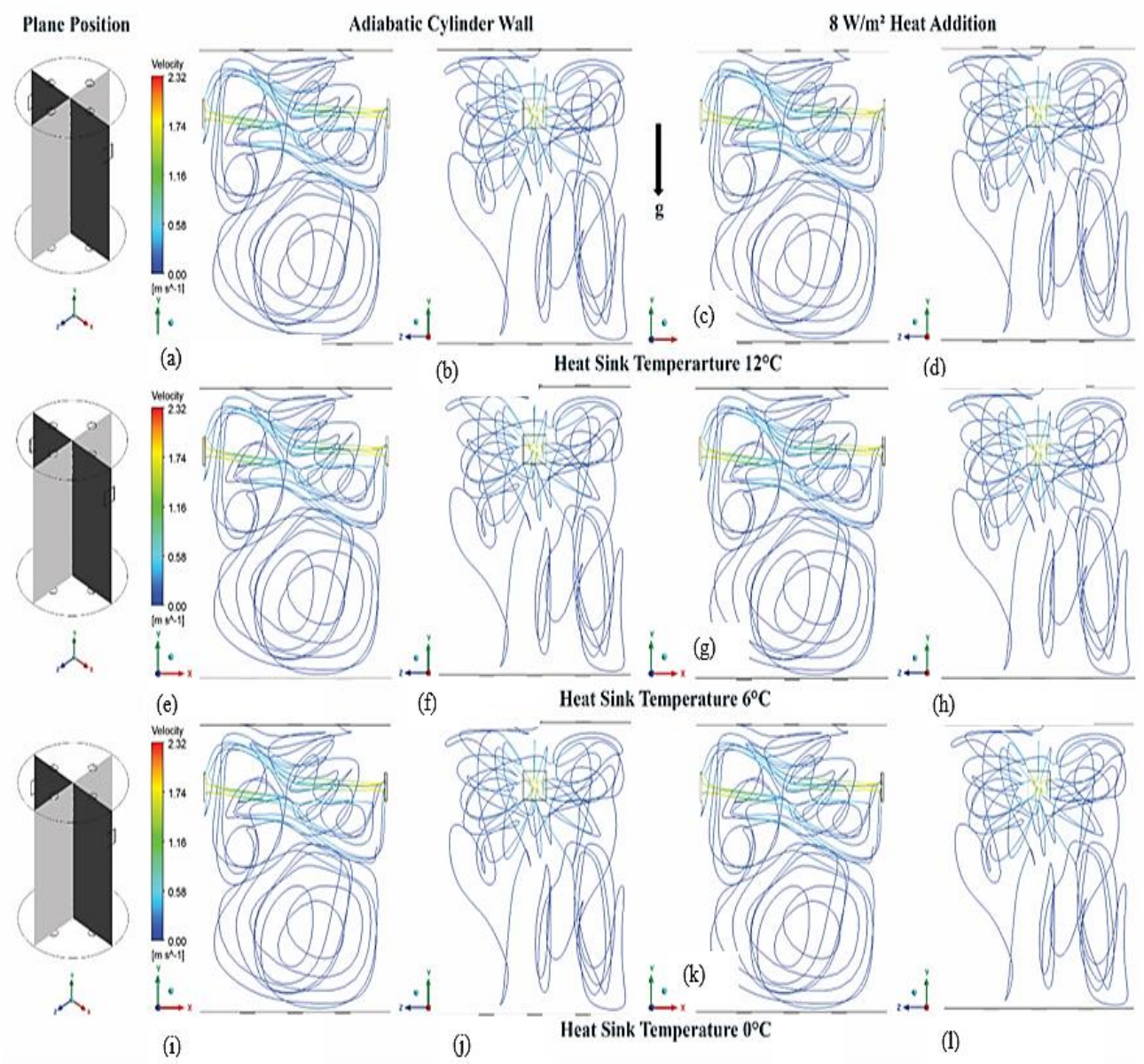

Fig. 9 Streamlines of airflow within the enclosure for case 1 vertically oriented heat sink

determined to be 0.52×10^{-3} kg/s, which is an average of 13 air exchanges per hour for this enclosure.

Figure 10-a-f shows that the air streams from the two fans keep oscillating either towards the bottom left of the enclosure or towards the bottom right of the enclosure at different instants of time.

This is commonly observed in buoyancy-driven flow problems due to the small density gradients, fluid inertia, and viscous forces (Bharadwaj & Das, 2017; Kulkarni et al., 2018; Joshi & Patil, 2019).

These oscillations are necessary for air exchange through vent holes. Without the oscillations, there can be no air exchange through the vent holes, and the holes essentially behave as walls. Figure 12-13 shows the Grashoff number (Gr) contour plots at different time intervals at the central XY plane for the Case 1-T0-q0 and

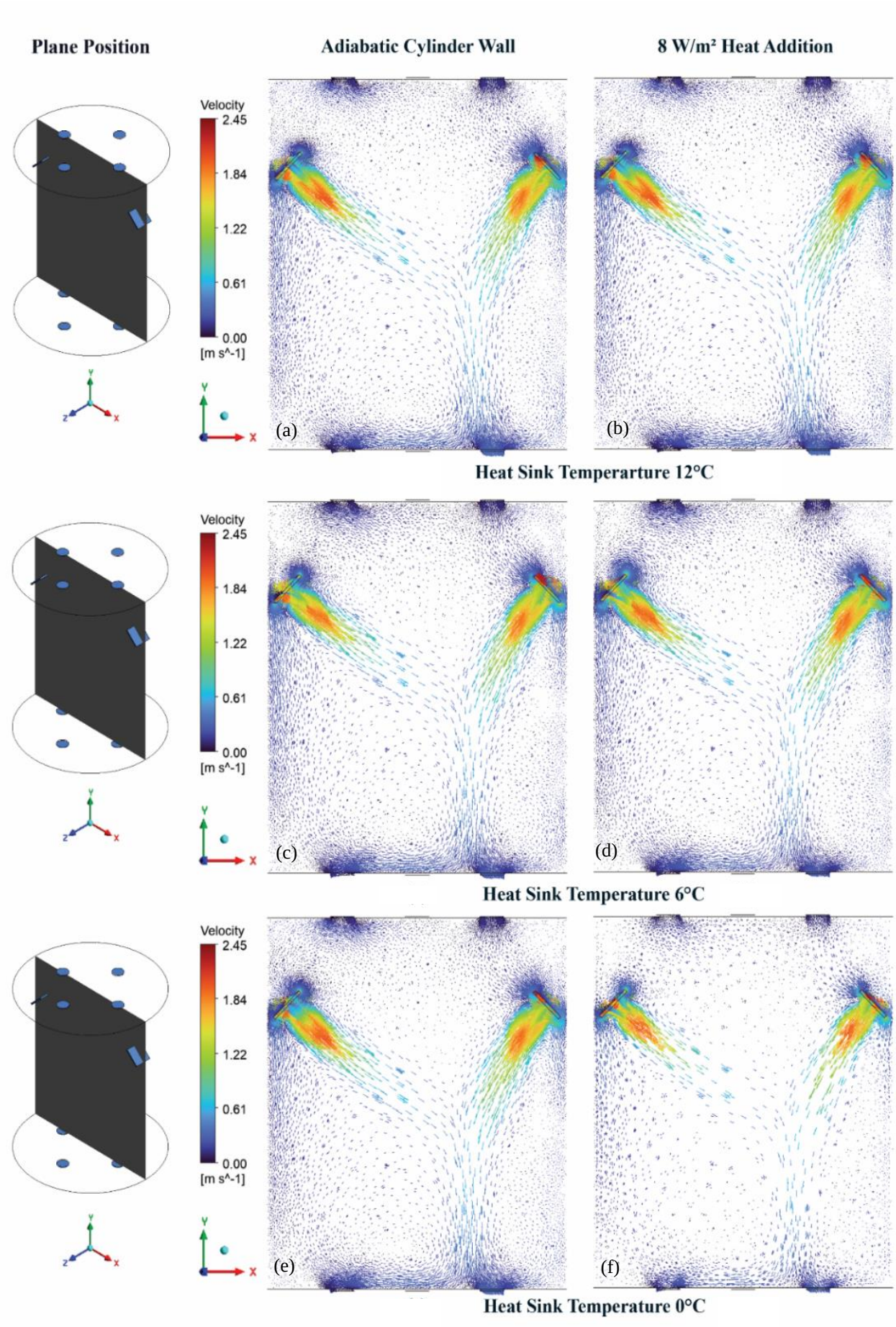

Fig. 10 Velocity vector plot of the case 2 inclined heat sink

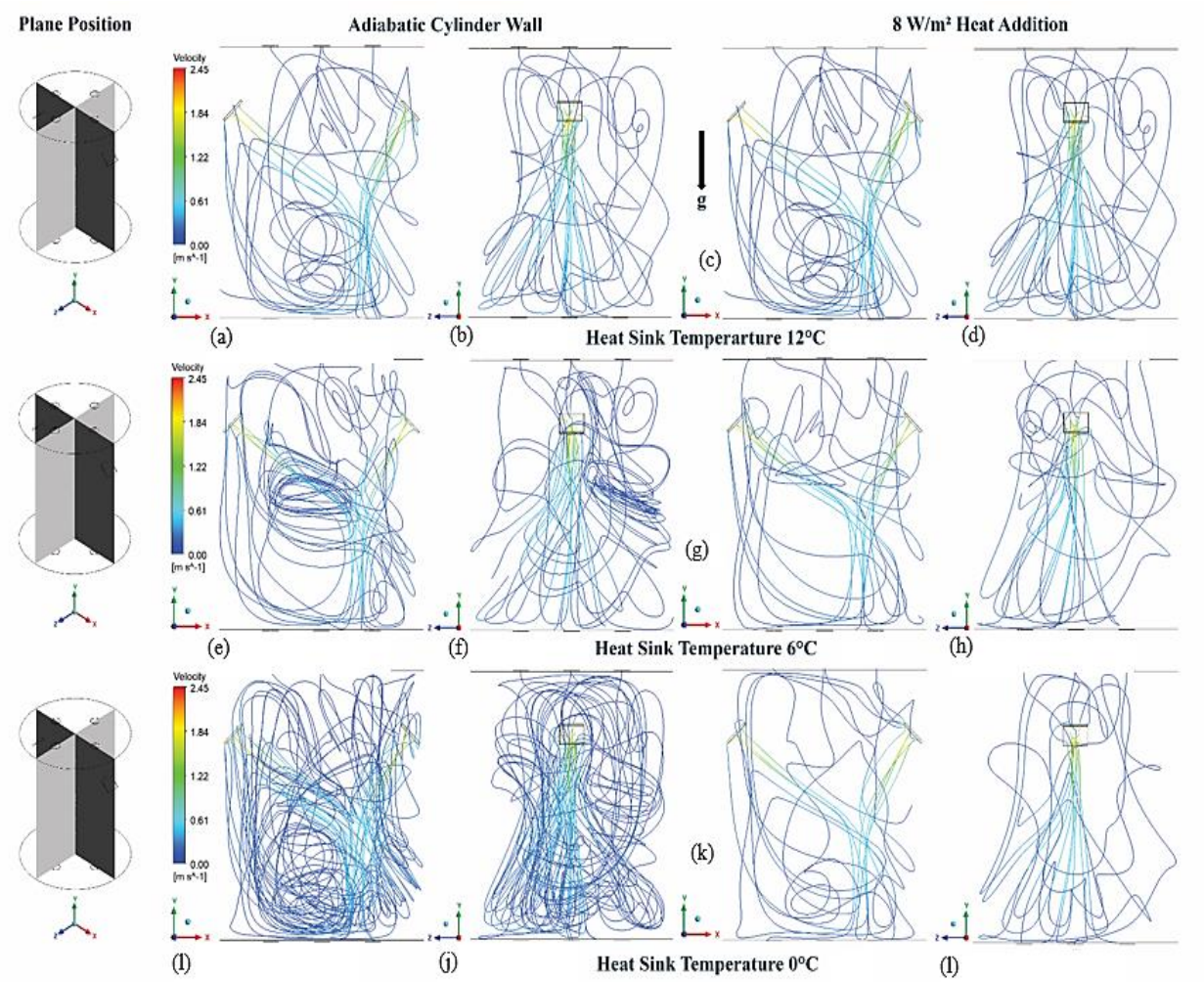

Fig. 11 Streamlines of airflow within the enclosure for the case 2 inclined heat sink

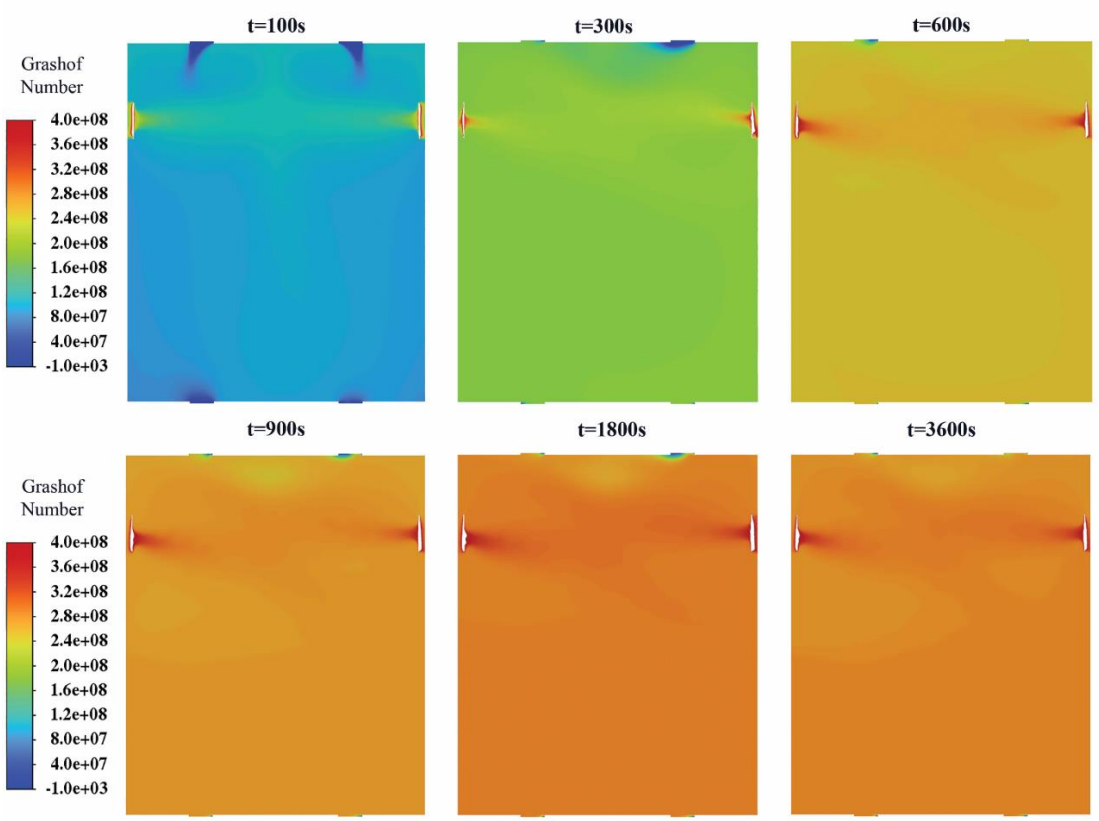

Fig. 12 Grashof number plot at different times of Case 1-T0-q0 configuration

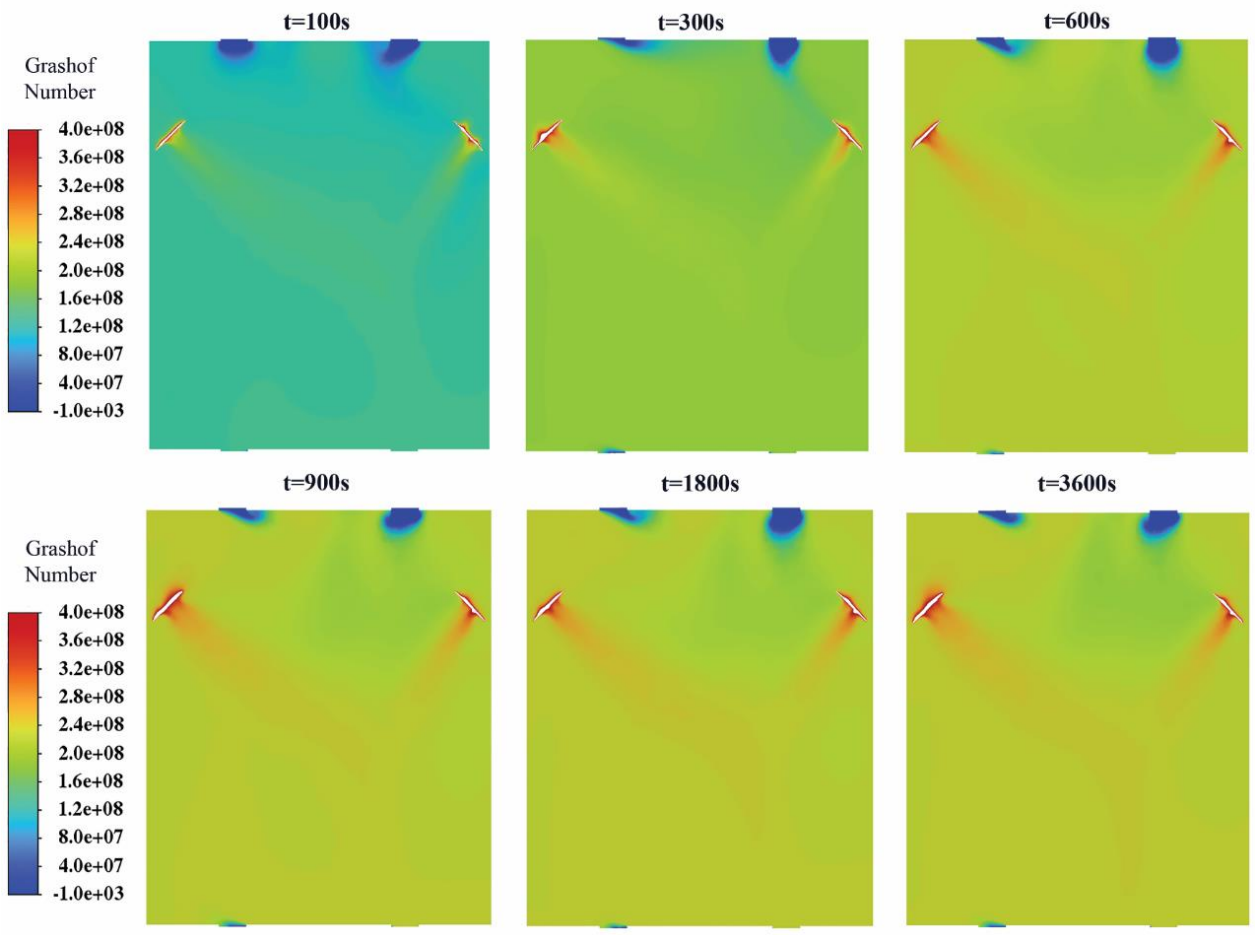

Fig. 13 Grashof number plot at different times of Case 2-T0-q0 configuration

Case 2-T0-q0 configurations, respectively. Gr compares the buoyancy forces with the viscous forces generated in a free convection flow. Typically, the instabilities are set in if the Gr > 10^3 (Adrian, 2013). Figure 12 and 13 show a rise in Gr from t = 100s to t = 3600s, with no significant change observed after t=900s. This points to the instabilities set in the enclosure after t = 900s. These instabilities promoted air exchange. In the present analysis, the average Gr of the order of 10^7. The minimum Gr was observed near the vent holes, while the maximum was near the heat sink surfaces. Figure 14-15 shows the Grashoff number (Gr) contour plots of all studied configurations at the central XY plane. The interpretation of these contour plots has shown that the range of Gr variations is higher with lower heat sink surface temperature and with adiabatic sidewalls.

Figure 16 presents the range of T_{air} observed inside the enclosure with 8 W/m^2 heat flux from the sidewalls for case 1 and case 2. We observed a reduction in the enclosure's T_{air} of approximately 3°C, 3-6°C, and 4-7°C, with the T_{sink} set at 12°C, 6°C, and 0°C respectively, and surrounding T_{air} at 37°C. This temperature range is ideal for crops like Groundnut (Sanjel et al., 2024), and mango (Espínola Sobrinho et al., 2004) during their different growth stages. However, the sink inclination is essential in locating the soil compost inside the enclosure. Crops in a relatively cold environment require perfect insulation for the enclosure. The ability of the enclosure to maintain a steady temperature mostly depends on the insulation material used. Hence, it is essential to look for thick insulation to avoid heat flux from the sidewall. Figure 17 illustrates the range of T_{air} achievable within the enclosure when the sidewall is adiabatic. The inclination of the heat sink surface significantly impacts the T_{air}. Inclined heat sinks with adiabatic sidewalls resulted in temperature reductions of 8-10°C, 9-12°C, and 11-15°C, respectively, with 12°C, 6°C, and 0°C heat sink surface temperatures.

On the other hand, the vertical heat sink could result in temperature reductions by 10-13°C, 12-16°C, and 15-19°C. Suitable crop and enclosure configurations can be planned for cultivation based on the desired thermal environment. The required air exchange rate should also be considered when choosing the configuration. With this second set of configurations, one can grow Cauliflower, Eggplants, Tomato, Cucumber, Green beans, Pepper, Rose flowers (Mostafavi & Rezaei, 2019), Garlic (Wu et al., 2016), Onion (Ratnarajah & Gnanachelvam, 2021), and Maize (Hou et al., 2014), Mustard (Kayaçetın et al., 2019) in a single room relatively at a higher temperature like 37°C, the temperature value that was set in the simulations.

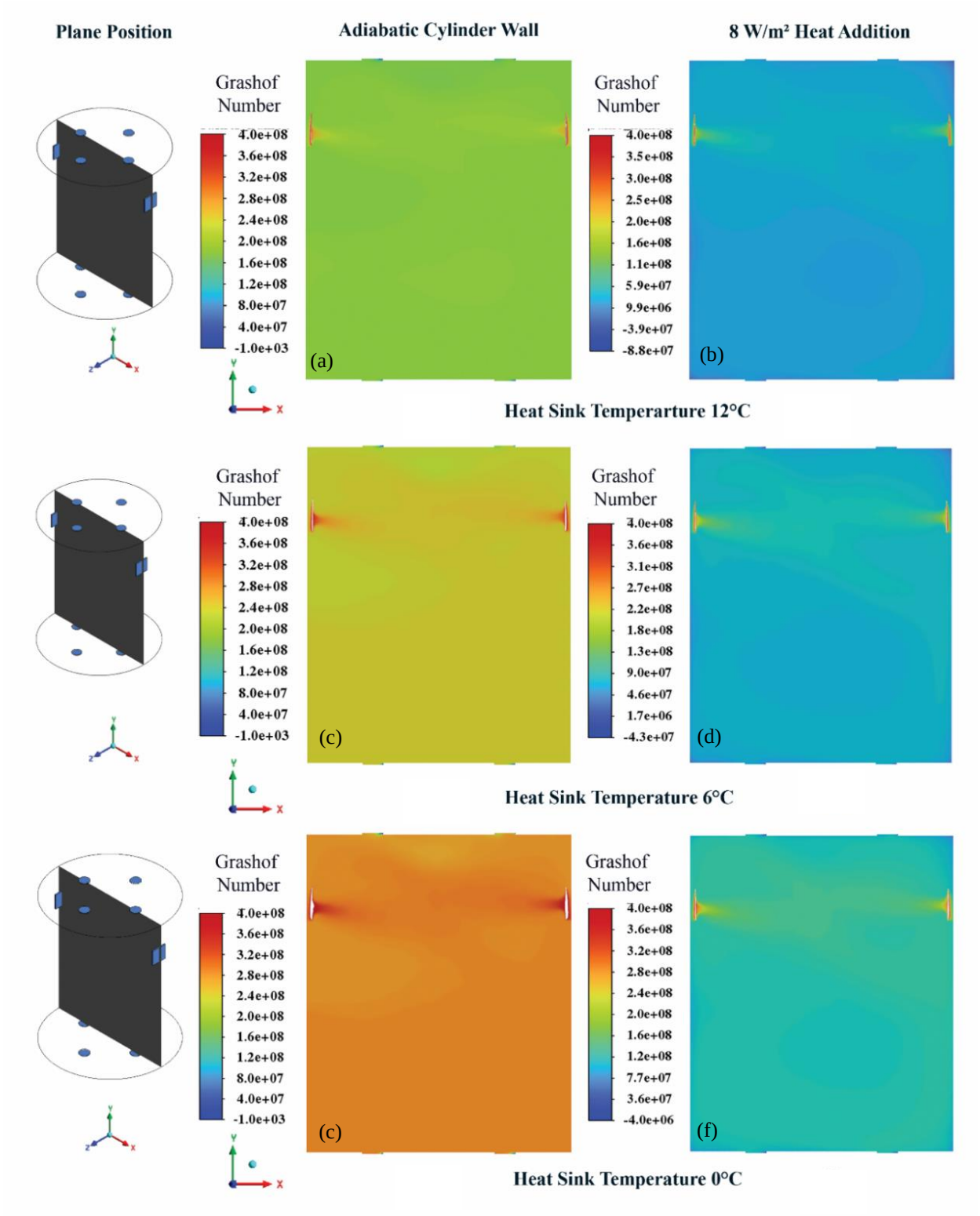

Fig. 14 Grashof Number contour plot for the vertical heat sink configurations

The given enclosure configurations have been proven to possess the capability to effectively regulate air temperatures within a confined space while facilitating air exchange. This feature is essential to create optimal micro-climatic conditions required for plant growth. Therefore, these enclosures can be utilized as standalone units within a designated area to establish distinct micro-climatic conditions (thermal zones) in a confined space.

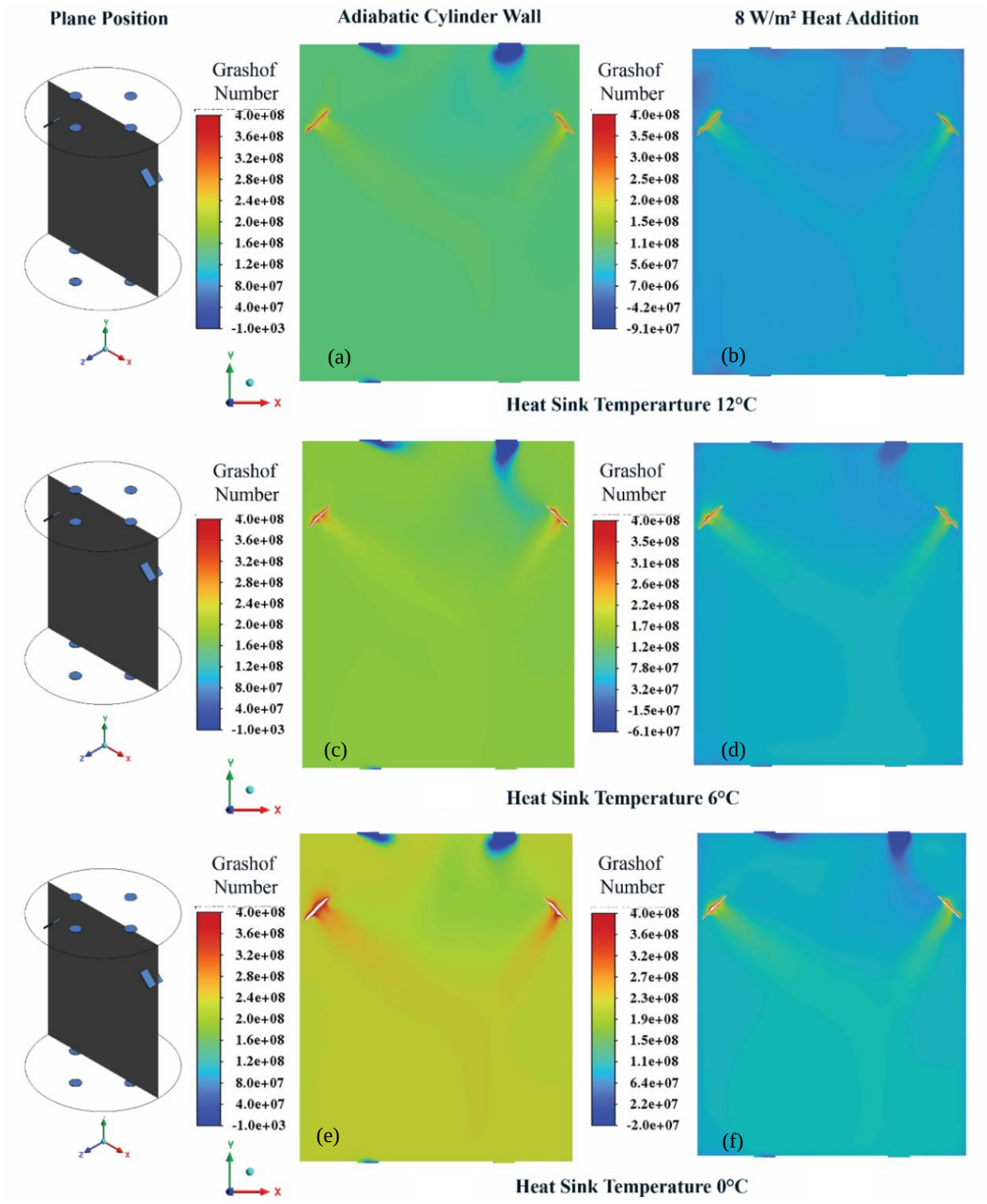

Fig. 15 Grashof Number contour plot for the inclined heat sink configurations

This level of control over micro-climatic conditions is not easily achievable with conventional centralized air conditioning systems. Furthermore, as previously mentioned, these enclosures consume less energy compared to air conditioning and are cost-effective.

4. CONCLUSION

Creating multiple thermal zones in a single room can be beneficial for indoor farming and research. This allows for cultivating a wide range of plants and facilitates scientific investigations. Various configurations are available for vented enclosures, including those with vertical and inclined heat sinks and options with or without heat flux from the sidewall. Nevertheless, the ability to create multiple thermal zones is significant, as it provides varying thermal environments within the enclosure while still facilitating air exchange. Case 2 with a 45° inclined heat sink orientation may be preferred if a cold air stream is needed over the crop.

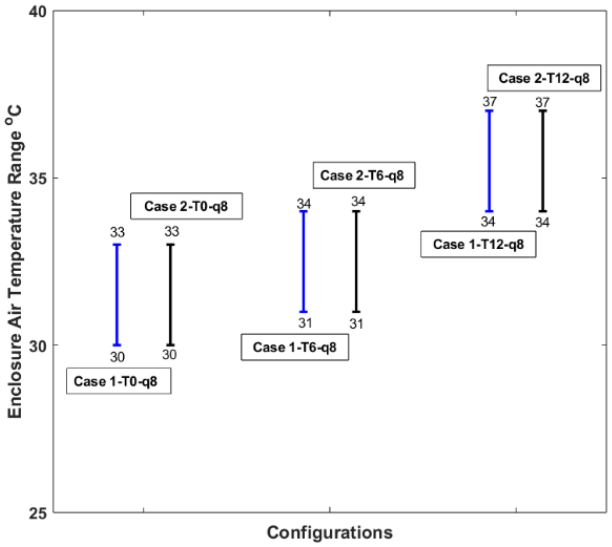

Fig. 16 Comparison of enclosure air temperature range of case 1 vertical heat sink and case 2 inclined heat sink configurations for 8 W/m^2 heat flux from the enclosure wall

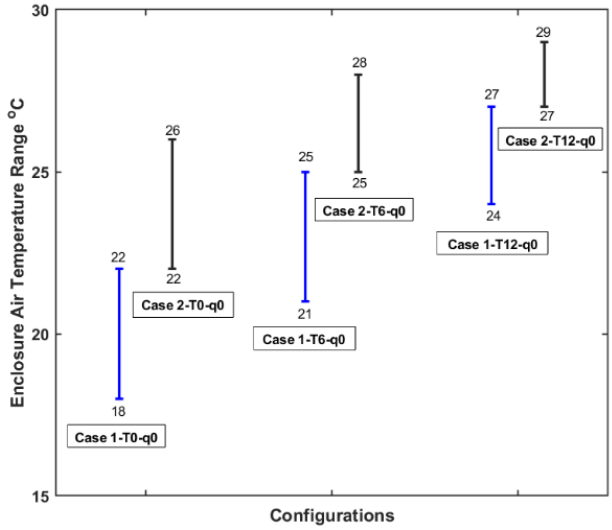

Fig. 17 Comparison of enclosure average air temperature range of case 1 and case 2 configurations for an adiabatic enclosure wall

On the other hand, if a region of still air is needed in the core region of the enclosure, case 1 with a vertically oriented heat sink may be preferred. Proper air circulation within the enclosure is crucial for maximizing energy plots indicate that the mixing was adequate in all configurations involving an inclined heat sink. efficiency in air cooling systems. The streamlines and vector. The calm areas noticed in vertical heat sink scenarios serve different functions, such as the placement of soil compost. Understanding the instabilities in the buoyancy-driven flow is crucial for optimizing air exchange through the vent holes of the enclosure. Considering the construction of the sidewall using Styrofoam, a thermal insulator, it is essential to factor in the heat flux from the sidewall, as it greatly affects the air temperature.

ACKNOWLEDGEMENTS

This work is funded by VIT, Vellore University, under VIT seed grant funds SG20230074 and 2641.

CONFLICT OF INTEREST

The author declares that there is no conflict of interest.

AUTHORS CONTRIBUTION

All three authors have made significant contributions to experimental investigation, research methodology, data curation, formal analysis, writing-original draft preparation, and critical revision of the article.

REFERENCES

Adrian, B. (2013). *Convection Heat Transfer* (4th ed.). Wiley. https://doi.org/10.1002/9781118671627

Afshari, F. (2021). Experimental and numerical investigation on thermoelectric coolers for comparing air-to-water to air-to-air refrigerators. *Journal of Thermal Analysis and Calorimetry*, *144*(3), 855–868. https://doi.org/10.1007/s10973-020-09500-6

Afshari, F., Mandev, E., Muratçobanoğlu, B., Yetim, A. F., & Ceviz, M. A. (2023). Experimental and numerical study on a novel fanless air-to-air solar thermoelectric refrigerator equipped with boosted heat exchanger. *Renewable Energy*, *207*(February), 253–265. https://doi.org/10.1016/j.renene.2023.02.092

Ashrae (2021). *Fundamentals* (SI Edition). American Society of Heating, Refrigerating and Air-Conditioning Engineers, Inc. (ASHRAE), US. https://www.ashrae.org/technical-resources/ashrae-handbook/description-2021-ashrae-handbook-fundamentals

Astrain, D., Vián, J. G., & Albizua, J. (2005). Computational model for refrigerators based on Peltier effect application. *Applied Thermal Engineering*, *25*(17–18), 3149–3162. https://doi.org/10.1016/j.applthermaleng.2005.04.003

Bharadwaj, K. K., & Das, D. (2017). Global instability analysis and experiments on buoyant plumes. *Journal of Fluid Mechanics*, *832*, 97–145. https://doi.org/10.1017/jfm.2017.665

Bhattacharya, P., & Das, S. (2015). A study on steady natural convective heat transfer inside a square cavity for different values of rayleigh and nusselt numbers. *Journal of Applied Fluid Mechanics*, *8*(3), 635–640. https://doi.org/10.18869/acadpub.jafm.67.222.22837

Bouras, A., Bouabdallah, S., Ghernaout, B., Arıcı, M., Cherif, Y., & Sassine, E. (2021). 3D numerical simulation of turbulent mixed convection in a cubical cavity containing a hot block. *Journal of Applied Fluid Mechanics*, *14*(6), 1869–1880.

https://doi.org/10.47176/JAFM.14.06.32604

Daimon, S., Iguchi, R., Hioki, T., Saitoh, E., & Uchida, K. I. (2016). Thermal imaging of spin Peltier effect. *Nature Communications*, *7*, 1–7. https://doi.org/10.1038/ncomms13754

Dimova, V., Georgiev, D., Georgiev, R., & Grigorov, S. (2020). Design of an energy efficient building equipped with air conditioning system for growing "kladnitsa" mushrooms. *Bulgarian Journal of Agricultural Science*, *26*, 221–228. https://www.agrojournal.org/26/01s-29.pdf

Engler, N., & Krarti, M. (2021). Review of energy efficiency in controlled environment agriculture. *Renewable and Sustainable Energy Reviews*, *141*(February), 110786. https://doi.org/10.1016/j.rser.2021.110786

Espínola Sobrinho, J., Menezes, J. B., Leitão, M. M. V. B. R., Souza, T. H., Melo, F. C., & Machado, F. L. C. (2004). Effect of air temperature on mango tree yield and fruit quality. *Acta Horticulturae*, *645*, 189–194. https://doi.org/10.17660/ActaHortic.2004.645.16

Evans, J. A., Foster, A. M., Huet, J. M., Reinholdt, L., Fikiin, K., Zilio, C., Houska, M., Landfeld, A., Bond, C., Scheurs, M., & Van Sambeeck, T. W. M. (2014). Specific energy consumption values for various refrigerated food cold stores. *Energy and Buildings*, *74*(2014), 141–151. https://doi.org/10.1016/j.enbuild.2013.11.075

Fordham, R., & Hadley, P. (2003). Cabbage and related vegetables. *Encyclopedia of Food Sciences and Nutrition*, 5932–5936. https://doi.org/10.1016/B0-12-227055-X/01234-7

Hou, P., Liu, Y., Xie, R., Ming, B., Ma, D., Li, S., & Mei, X. (2014). Temporal and spatial variation in accumulated temperature requirements of maize. *Field Crops Research*, *158*(June 2022), 55–64. https://doi.org/10.1016/j.fcr.2013.12.021

Ibikunle, R. A., Akintunde, M. A., Titiladunayo, I. F., & Adeleke, A. A. (2022). Estimation of coefficient of performance of thermoelectric cooler using a 30 W single-stage type. *International Review of Applied Sciences and Engineering*, *13*(2), 124–132. https://doi.org/10.1556/1848.2021.00322

Iyi, D., Hasan, R., & Penlington, R. (2018). Experimental and numerical study of Buoyancy-driven low turbulence flow in rectangular enclosure partially filled with isolated solid blockages. *International Journal of Heat and Mass Transfer*, *127*, 534–545. https://doi.org/10.1016/j.ijheatmasstransfer.2018.07.031

Joshi, V. V., & Patil, S. (2019). Heat transfer enhancement in a calandria based reactor with a new inlet design - A CFD analysis. *Journal of the Chinese Society of Mechanical Engineers, Transactions of the Chinese Institute of Engineers, Series C/Chung-Kuo Chi Hsueh Kung Ch'eng Hsuebo Pao*, *40*(3), 299–306. https://journal.csme.org.tw/vol_file.aspx?lang=en&fid=20210505134215

Kayaçetın, F., Onemlı, F., Yilmaz, G., Khaward, K. M., Kinay, A., Hatıpoğlu, H., Kivilcimf, M. N., Kara, N., Köse, A., Sefaoğlu, F., & Ozaydina, K. A. (2019). Growing degree day and seed yield relationships in mustard (*Brassica juncea* L.) under different sowing seasons and locations of Turkey. *Tarim Bilimleri Dergisi*, *25*(3), 298–308. https://doi.org/10.15832/ankutbd.424218

Khan, F., & Chandra, R. (2017). Effect of physiochemical factors on fruiting body formation in mushroom. *International Journal of Pharmacy and Pharmaceutical Sciences*, *9*(10), 33–36. https://doi.org/10.22159/ijpps.2017v9i10.20086

Kulkarni, P. S., Rajan, N. K. S., Suneel, M. P., & Joshi, V. (2018). *Fluid flow and heat transfer analysis in a calandria based reactor for different fuel channel configurations*. 10th International Conference on Computational Fluid Dynamics, ICCFD 2018 - Proceedings, 1–9. https://www.iccfd.org/iccfd10/papers/ICCFD10-270-Paper.pdf

Kumar, A., & Subudhi, S. (2020). Thermal fluctuations and boundary layer properties of turbulent natural convection inside open cavities of different dimensions heated from below. *Physics of Fluids*, *067114*(32), 067114-(1-12). https://doi.org/10.1063/5.0008160

Lakhiar, I. A., Gao, J., Syed, T. N., Chandio, F. A., & Buttar, N. A. (2018). Modern plant cultivation technologies in agriculture under controlled environment: A review on aeroponics. *Journal of Plant Interactions*, *13*(1), 338–352. https://doi.org/10.1080/17429145.2018.1472308

Morgan, R. G., Ibarra, R., Zadrazil, I., Matar, O. K., Hewitt, G. F., & Markides, C. N. (2017). On the role of buoyancy-driven instabilities in horizontal liquid–liquid flow. *International Journal of Multiphase Flow*, *89*, 123–135. https://doi.org/10.1016/j.ijmultiphaseflow.2016.07.009

Mostafavi, S. A., & Rezaei, A. (2019). Energy consumption in greenhouses and selection of an optimized heating system with minimum energy consumption. *Heat Transfer - Asian Research*, *48*(7), 3257–3277. https://doi.org/10.1002/htj.21540

Netam, R. S., Yadav, S. C., Mukherjee, S. C., & Kumari, P. (2018). Cultivation of button mushroom (*Agaricus bisporus*) under controlled condition: An initiative in bastar plateau of chhattisgarh. *International Journal of Current Microbiology and Applied Sciences*, *7*(10), 782–787. https://doi.org/10.20546/ijcmas.2018.710.087

Pasapuleti, P., Reddy Siddavatam, A. K., & Krishnamoorthy, H. S. (2022). *Net-zero-energy based sustainable agriculture: A case study of container mushroom farming*. 10th IEEE International Conference on Power Electronics, Drives and Energy Systems, PEDES. https://doi.org/10.1109/PEDES56012.2022.1008053

8

Plouraboué, F., Rudkiewicz, M., David, F., Neau, H., & Debenest, G. (2024). Natural convective loops heat transfer scaling analysis. *International Journal of Heat and Mass Transfer*, *218*(September 2023), 124743. https://doi.org/10.1016/j.ijheatmasstransfer.2023.124743

Ratnarajah, V., & Gnanachelvam, N. (2021). Effect of Abiotic Stress on Onion Yield: A Review. *Advances in Technology*, *1*(1), 147–160. https://doi.org/10.31357/ait.v1i1.4876

Revathi, S., Sivakumaran, N., & Radhakrishnan, T. K. (2019). Design of solar-powered forced ventilation system and energy-efficient thermal comfort operation of greenhouse. *Materials Today: Proceedings*, *46*, 9893–9900. https://doi.org/10.1016/j.matpr.2021.01.409

Rubatzky, V. E., & Yamaguchi, M. (2012). *World vegetables: principles, production, and nutritive values*. Springer Science & Business Media. Springer Science & Business Media. https://doi.org/10.1007/978-94-011-7907-2

Rudresha, N., Vijay Kumar, M., & Math, M. M. (2023). A parametric study and performance investigation of thermoelectric refrigeration system using computational fluid dynamics. *International Journal of Air-Conditioning and Refrigeration*, *31*(1). https://doi.org/10.1007/s44189-023-00031-x

Sanjel, S., Colee, J., Barocco, R. L., Dufault, N. S., Tillman, B. L., Punja, Z. K., Seepaul, R., & Small, I. M. (2024). Environmental factors influencing stem rot development in peanut: predictors and action thresholds for disease management. *Phytopathology*, *114*(2), 393–404. https://doi.org/10.1094/PHYTO-05-23-0164-R

Sheikholeslami, M., & Khalili, Z. (2024a). Environmental and energy analysis for photovoltaic-thermoelectric solar unit in existence of nanofluid cooling reporting CO_2 emission reduction. *Journal of the Taiwan Institute of Chemical Engineers*, *156* (December 2023), 105341. https://doi.org/10.1016/j.jtice.2023.105341

Sheikholeslami, M., & Khalili, Z. (2024b). Solar photovoltaic-thermal system with novel design of tube containing eco-friendly nanofluid. *Renewable Energy*, *222*(December 2023), 119862. https://doi.org/10.1016/j.renene.2023.119862

Singh, A. K., & Singh, A. K. (2019). Influence of heat and mass transfer on free convection of micropolar fluid between vertical concentric cylinders. *Journal of Applied Fluid Mechanics*, *12*(5), 1539–1545. https://doi.org/10.29252/jafm.12.05.29040

Söylemez, E., Alpman, E., Onat, A., & Hartomacıoğlu, S. (2021). CFD analysis for predicting cooling time of a domestic refrigerator with thermoelectric cooling system. *International Journal of Refrigeration*, *123*, 138–149. https://doi.org/10.1016/j.ijrefrig.2020.11.012

Söylemez, E., Alpman, E., Onat, A., Yükselentürk, Y., & Hartomacıoğlu, S. (2019). Numerical (CFD) and experimental analysis of hybrid household refrigerator including thermoelectric and vapour compression cooling systems. *International Journal of Refrigeration*, *99*, 300–315. https://doi.org/10.1016/j.ijrefrig.2019.01.007

Weidner, T., Yang, A., & Hamm, M. W. (2021). Energy optimisation of plant factories and greenhouses for different climatic conditions. *Energy Conversion and Management*, *243*(April), 114336. https://doi.org/10.1016/j.enconman.2021.114336

Wen, X., Wang, L. P., & Guo, Z. (2021). Development of unsteady natural convection in a square cavity under large temperature difference. *Physics of Fluids*, *33*(8). https://doi.org/10.1063/5.0058399

Wu, C., Wang, M., Cheng, Z., & Meng, H. (2016). Response of garlic (Allium sativum L.) bolting and bulbing to temperature and photoperiod treatments. *Biology Open*, *5*(4), 507–518. https://doi.org/10.1242/bio.016444.